Philosophical Magazine
Publication details, including instructions for authors and subscription information:
http://www.tandfonline.com/loi/tphm20

γ-precipitate strengthening in nickel-based superalloys

Akiyuki Takahashi [a] , Mitsuru Kawanabe [a] & Nasr M. Ghoniem [b]
[a] Department of Mechanical Engineering, Faculty of Science and Technology, Tokyo University of Science, 2641 Yamazaki, Noda-shi, Chiba 278-8510, Japan
[b] Department of Mechanical and Aerospace Engineering, University of California, Los Angeles, Los Angeles, CA 90095

Available online: 13 Jul 2010

To cite this article: Akiyuki Takahashi, Mitsuru Kawanabe & Nasr M. Ghoniem (2010): γ-precipitate strengthening in nickel-based superalloys, Philosophical Magazine, 90:27-28, 3767-3786

To link to this article: http://dx.doi.org/10.1080/14786435.2010.497470

Philosophical Magazine
Vol. 90, Nos. 27–28, 21–28 September 2010, 3767–3786

γ-precipitate strengthening in nickel-based superalloys

Akiyuki Takahashi[a]*, Mitsuru Kawanabe[a] and Nasr M. Ghoniem[b]

[a]*Department of Mechanical Engineering, Faculty of Science and Technology, Tokyo University of Science, 2641 Yamazaki, Noda-shi, Chiba 278-8510, Japan;* [b]*Department of Mechanical and Aerospace Engineering, University of California, Los Angeles, Los Angeles, CA 90095*

(*Received 20 April 2009; final version received 24 May 2010*)

We describe here a computational method to study γ-precipitate strengthening in nickel-based superalloys, and to specifically investigate the relative importance of stacking-fault energy and coherency strains. The method is a combination of the Parametric Dislocation Dynamics (PDD), an analytical solution to the spherical inclusion problem and the generalized Peierls–Nabarro (P-N) model. Earlier analytical solutions to stacking-fault strengthening predict a lower critical resolved shear stress (CRSS) in comparison with the results of the present model. This is attributed to shape changes of super-dislocations during their interaction with γ-precipitates. However, existing analytical solutions to coherency strengthening provide considerably larger values of the CRSS compared with the results of present simulations. The dislocation core is found to spread widely as it interacts with γ-precipitates, and is thus much softer than what has been considered in previous analytical solutions. This remarkable effect is a direct result of the core structure of dislocations interacting with precipitates. When this effect is accounted for, a new analytical solution is shown to give excellent agreement with present simulation results. We finally discuss the combined effects of the two strengthening mechanisms, when they operate simultaneously.

Keywords: generalized Peierls–Nabarro model; dislocation dynamics; Ni-based superalloys; precipitation

1. Introduction

Precipitation strengthening is one of the most effective techniques to design alloys for a desired combination of strength and ductility. The main mechanism of strengthening is generally known to be the interaction between dislocations and precipitates, where precipitates impede the motion of dislocations, resulting in an increase in the flow stress and a corresponding change in ductility. The classical theory of precipitation strengthening is already well established on the basis of dislocation–precipitate interaction mechanisms, and provides useful information for practical alloy design [1]. Precipitation strengthening is categorized into elementary contributing mechanisms; such as changes in the stacking-fault energy, effects of

*Corresponding author. Email: takahash@rs.noda.tus.ac.jp

ISSN 1478–6435 print/ISSN 1478–6443 online

DOI: 10.1080/14786435.2010.497470
http://www.informaworld.com

coherency strains, effects of elastic modulus mismatch between the matrix and precipitate, and the influence of precipitate crystal structure in relation to the matrix. The primary objective of the theory is to provide an accurate evaluation of the critical resolved shear stress (CRSS), and its dependence on the individual mechanisms.

Hirsch and Kelly proposed an analytical equation for the dependence of the CRSS on the stacking-fault energy, and discussed the influence of the difference between the stacking-fault energy of the matrix and that of the precipitate [2]. They used an extended dislocation model, where the dislocation was represented by two partial dislocations and a stacking-fault in-between. Nembach modified this solution, and developed another equation for accurate evaluation of the CRSS [3]. On the other hand, Gerold and Haberkorn pursued an analytical study of coherency strain strengthening, and proposed an equation for its contribution to the CRSS [4]. They assumed a spherical precipitate with a coherency strain, where the elastic field impedes dislocation motion, either inside the precipitate or in the matrix. All these analytical approaches capture the qualitative behavior of the CRSS. However, quantitative evaluation of the CRSS as a result of precipitate strengthening necessitates that the assumptions involved in analytical estimates should be removed. In analytical approximations, the dislocation is assumed to be straight, and the dislocation core structure is ignored. Therefore, to provide quantitative evaluations of precipitate strengthening, we must examine the influence of the dislocation line flexibility, and the role that the dislocation core structure plays during its interaction with precipitates. Analytical equations can then be revised on the basis of detailed numerical calculations, when necessary.

One of the interesting applications is the strengthening caused by precipitation in nickel-based superalloys. These alloys have been extensively investigated, because $L1_2$-type long-range ordered intermetallic compounds, such as Ni_3Al, Ni_3Si and Co_3Ti, are considered for high-temperature structural applications. Miller observed extensive formation of spherical γ-precipitates in the γ' matrix phase of a nickel-based superalloy using 3-D atom probe measurements [5]. Nemoto et al. measured the increase in the yield strength of the alloy resulting from the formation of γ-precipitates, and provided a clear picture of the influence of γ-precipitate strengthening on the inverse temperature dependence of the yield strength of the alloy [6]. Thus, understanding the role of γ-precipitates on alloy strength, and the detailed mechanisms involved during the interaction between a dislocation and γ-precipitates is fundamental to the control and improvement of the mechanical properties.

Recently, computer simulation techniques have provided an opportunity to investigate the detailed mechanisms of material deformation without many of the assumptions that must be invoked in order to develop analytical approaches. The dislocation dynamics (DD) computer simulation technique has been developed to study metal deformation from a fundamental perspective, as the method allows simulation of the collective behavior of dislocation ensembles, and to derive the macroscopic deformation response on the basis of dislocation mechanisms [7]. However, the original development of the DD technique was based on elasticity solutions for dislocations in an infinite medium, without the influence of external or internal surfaces. Subsequently, Van der Giessen and Needleman utilized the

superposition principle to account for the geometry of the material in two-dimensional DD simulations [8], employing the finite element method (FEM) to solve the correction problem arising from the application of the superposition principle. Weygand et al. extended the method to three-dimensional DD simulations [9]. More recently, Takahashi and Ghoniem extended the superposition principle to general three-dimensional dislocation–precipitate interaction problems [10]. They derived a set of boundary-volume integral equations for the correction problem, and solved the equations using the boundary element method (BEM) with a volume integral term. The method allows us to deal with flexible dislocation lines, and can thus give important information on the influence of dislocation shape change on its interaction with precipitates. Xiang et al. developed a level set method to simulate the dynamics of dislocations. They simulated the complex dislocation behavior in the vicinity of spherical inclusions including the cross-slip of screw parts of the dislocation [11]. Devicre et al. developed a discrete continuous model (DCM), where the dislocations are represented as eigenstrains in the continuum calculation using the FEM, and the dynamics of dislocations is calculated based on the FEM result of the stress calculation. Using the DCM method, they calculated and discussed the critical stress for dislocations to move the $\gamma'/\gamma/\gamma'$ channel [12]. Rao et al. investigated the interaction between dislocations and both γ- and γ'-precipitates using the DD method [13]. They studied the dependence of the CRSS on the shape and volume fraction of the γ-precipitates. However, these studies did not deal with an extended dislocation core structure, and hence it is clearly necessary to implement a new idea that can incorporate the dislocation core structure into DD simulations. Banerjee et al. developed a generalized Peierls–Nabarro (GPN) model to determine the dislocation core structure, taking into account crystal lattice resistance to slip through *ab initio* calculations, and also generalizing the dislocation shape as a 3-D space curve [14]. The main idea is to descritize the elastic interaction part of the equation with a number of fractional dislocations having small Burgers vectors. The lattice restoring part of the force equilibrium equation is evaluated taking the derivative of the γ-surface energy obtained by separate *ab initio* calculations. They applied the method to static dislocation problems, and investigated the core structure of dislocation loops in f.c.c. metals.

The present model for the interaction between dislocations and precipitates has several advantages and a few limitations. First, in MD simulations, we cannot clearly separate the influence of the specific mechanisms on precipitation strengthening (e.g. the specific effects of stacking-fault energy, coherency strain, etc.). On the other hand, in the present model, it is very easy to add and delete the strengthening mechanisms, which provides an opportunity to understand the relative magnitude of strengthening mechanisms, as compared to classical precipitation theory. Second, the present model is not dependent on the accuracy of the interatomic potential used in MD simulations, because lattice resistance to dislocation motion is obtained from *ab initio* information. In particular, when we deal with new types of precipitates, we do not need to develop a valid interatomic potential for the matrix, precipitate, and their interaction zone, which is a significant task for each type of precipitate. And finally, the present model is not limited by the size of the MD simulation box, nor the boundary conditions used, which are usual limitations in many MD simulations.

Since the γ–γ' interface is coherent, restructuring of the dislocation core along this matrix–precipitate interface may not be significant. However, the present model must be extended to account for weak interfaces between precipitates and the matrix as discussed in the work of Shehadeh et al. [15]. To extend the present model to climbing dislocations (e.g. at high-temperature and under irradiation), we need to consider coupling between thermal/irradiation osmotic point defect forces and glide forces, which will move the dislocation out of the glide plane. However, the speed of dislocation glide is much faster than climb as a general rule, and thus we would expect that the effects of climb are small. This topic requires future modifications of the present model using kinetic information on defect fluxes generated by thermal or irradiation effects.

The objective of this paper is to develop and apply a computational method that can simulate the dislocation–precipitate interaction process, including the dynamics of the dislocation core itself. The development of this new computational procedure will be based on a combination of the Parametric Dislocation Dynamics (PDD) [7], and the GPN model [14]. Using the computational method, we will then simulate the interaction between a super-dislocation and a spherical γ-precipitate embedded in a γ'matrix of a nickel-based superalloy. The focus here will be an investigation of two main effects: (1) the influence of the dislocation line flexibility, and (2) the effects of the dislocation core structure on precipitation strengthening. We will examine, separately and in combination, the relative effects of changes in the stacking-fault energy between the precipitate and matrix, and the influence of coherency strains on the CRSS. On the basis of computer simulation results, we will revise the classical theoretical equations for coherency strengthening to account for the influence of the dislocation core structure, and we will show that classical analytical results extremely over-estimate the CRSS. Finally, we present results for precipitate strengthening, when stacking-fault and coherency strengthening are simultaneously operating together. In the next section, we present details of the computational method, followed by a description of the precipitate-dislocation model in Section 3. The results for stacking-fault and coherency strain strengthening are then presented in Section 4, while conclusions are finally drawn in Section 5.

2. Computational method

To determine the elastic interaction between precipitates and dislocations of an infinitesimal-size core, Takahashi and Ghoniem proposed a computational method, which is based on a combination of the original PDD method, and the BEM method [10]. On the other hand, the development of a GPN model by Banerjee et al. enables explicit representation of the core structure of dislocations within the PDD framework [14]. Thus, coupling between these two methods should open the door to investigations of the roles played by the dislocation line flexibility and its core structure on precipitation strengthening. In the following, we develop basic concepts for the elastic interaction between dislocations and precipitates. We also show how the PDD and the GPN methodologies can be combined.

2.1. *Solution to dislocation–precipitate elastic interaction problem*

Consider an infinite elastic body D, with elastic constants C_{ijkl}, containing N_p precipitates and N_d dislocations, and subjected to an external applied stress σ^0_{ij}. The mth precipitate, Ω^m, has elastic constants C^m_{ijkl}, and induces a coherency strain ϵ^m_{kl}. Following Mura [16], the stress in an infinite elastic body can be written as

$$\sigma^0_{ij} + \sigma_{ij} = \begin{cases} C_{ijkl}\left(\varepsilon^0_{kl} + \varepsilon_{kl}\right) & \text{in } D - \Omega \\ C^m_{ijkl}\left(\varepsilon^0_{kl} + \varepsilon_{kl} - \epsilon^m_{kl}\right) & \text{in } \Omega^m \end{cases}, \tag{1}$$

where $\varepsilon_{kl} = C^{-1}_{klij}\sigma^0_{ij}$, and Ω is the total volume occupied by N_p precipitates. Since it is difficult to solve Equation (1) directly, the superposition principle will be utilized in its solution:

$$\sigma^0_{ij} + \sigma_{ij} = \hat{\sigma}_{ij} + \tilde{\sigma}_{ij}, \tag{2}$$

where $\hat{\sigma}_{ij}$ is the stress in the elastic problem containing dislocations with an external applied stress, which is given as

$$\hat{\sigma}_{ij} = C_{ijkl}\left(\varepsilon^0_{kl} + \hat{\varepsilon}_{kl}\right). \tag{3}$$

The last equation can be solved using the PDD method. On the other hand, $\tilde{\sigma}_{ij}$ is a correction stress to the infinite medium solution, which should have an exact solution presented by Equation (1), when combined with Equation (3). Therefore, $\tilde{\sigma}_{ij}$ can be defined as

$$\tilde{\sigma}_{ij} = \begin{cases} C_{ijkl}\tilde{\varepsilon}_{kl} & \text{in } D - \Omega \\ C^m_{ijkl}\left(\tilde{\varepsilon_{kl}} - \epsilon^m_{kl}\right) + \left(C^m_{ijkl} - C_{ijkl}\right)\left(\varepsilon^0_{kl} + \tilde{\varepsilon}_{kl}\right) & \text{in } \Omega^m. \end{cases} \tag{4}$$

According to Equation (4), the correction field can be obtained from the solution of an inhomogeneous inclusion problem, with an initial stress $(C^m_{ijkl} - C_{ijkl})(\varepsilon^0_{kl} + \tilde{\varepsilon}_{kl})$ in the precipitates. Takahashi and Ghoniem derived boundary and volume integral equations for such an inhomogeneity problem (Equation (4)), and solved the boundary and volume integral equations using the BEM method, with a volume integral term. In the nickel-based superalloy γ-precipitate case, the elastic constants of both $\gamma'$and γ-phase are nearly the same, and thus the initial stress can be assumed to be zero. Then Equation (4) can be converted from the inhomogeneous inclusion problem to an inclusion problem. Additionally, if the shape of the precipitate is assumed to be an ellipsoid, the equation can be solved using the Eshelby tensor instead of the BEM method, which will drastically decrease the computational effort [17].

2.2. *Parametric dislocation dynamics method*

In the PDD method [7], flexible dislocation ensembles are discretized into a number of curved dislocation segments. The segments have two edge nodes, and the nodes have a generalized coordinate vector, which is a combination of position and tangent vectors. The curved shape of segments is represented by a cubic spline function that

can preserve high-order continuity conditions. The equation of motion of each dislocation ensembles is given by

$$\int_{\Gamma}\left(F_k - B_{\alpha k}\frac{\mathrm{d}Q_\alpha}{\mathrm{d}t}\right)\delta r_k|\mathrm{d}\mathbf{s}| = 0, \tag{5}$$

where F_k is the force per unit length of the dislocation, $B_{\alpha k}$ is the resistivity matrix and Q_k is the generalized coordinate for dislocations, which contains both position and tangent vectors at a given node of a dislocation. In this work, F_k is defined as

$$F_k = F_k^{\mathrm{ext}} + F_k^{\mathrm{int}} + F_k^{\mathrm{self}} + F_k^{\mathrm{ppt}}, \tag{6}$$

where F_k^{ext} is the force produced by the external stress, F_k^{int} is the interaction force with other dislocation loops, F_k^{self} is the self-force, and F_k^{ppt} is the force due to the elastic field generated by γ-precipitates. Integrating Equation (5), we can obtain the matrix form of the equation of motion for dislocation ensembles as

$$K_{ij}\frac{\mathrm{d}Q_j}{\mathrm{d}t} = F_i. \tag{7}$$

The dislocation velocity can be calculated by solving the above equation, and its time integration simulates the dynamical behavior of dislocations in response to external and internal stress fields. Details of the method can be found elsewhere [7].

2.3. *Elastic field of incoherent spherical γ-precipitates*

Since it is experimentally observed that most γ-precipitates in Ni-based superalloys have spherical or cuboidal shapes, we thus assume that the shape of the γ-precipitate is spherical, and utilize an analytical solution to the elastic field generated by the γ-precipitate [17]. The lattice constant of the γ-precipitate $a_0^{\gamma} = 0.352$ nm differs from that of the γ'-phase $a_0^{\gamma'} = 0.357$ nm. This difference provides a coherency strain $\in$ in the γ-precipitate, which is defined by

$$\in = \left(a_0^{\gamma} - a_0^{\gamma'}\right)/a_0^{\gamma'}. \tag{8}$$

As a result of Equation (8), the coherency strain is -0.0143. When the position of interest is inside the inclusion, the analytical solution to an elastic problem of a spherical inclusion with a coherency strain $\in$ is given by

$$\epsilon_r = \epsilon_t = \frac{1+\nu}{3(1-\nu)}\in, \tag{9}$$

where ν is Poisson's ratio, and ϵ_r and ϵ_t are the strain in the radial and tangential directions, respectively. On the other hand, when the point of interest is outside the inclusion, the strains are given by

$$\begin{aligned}\epsilon_r &= -\frac{2}{3}\frac{1+\nu}{1-\nu}\frac{a^3}{r^3}\in \\ \epsilon_t &= \frac{1}{3}\frac{1+\nu}{1-\nu}\frac{a^3}{r^3}\in,\end{aligned} \tag{10}$$

where a is the radius of the spherical inclusion, and r is the distance between the center of inclusion and the point of interest. The stress tensor at the point can then be easily calculated using Hooke's law, once the strain tensor is available.

2.4. *Dislocation core structure*

In the classical dislocation dynamics method, the character of dislocation lines is defined only by the line sense vector and the Burgers vector. However, the dislocation core structure is atomistic in nature, and hence cannot be accounted for in the classical dislocation dynamics method. To overcome this difficulty and to incorporate atomistic information into dislocation dynamic, the generalization of the original Peierls–Nabarro (P-N) model [18,19] by Banerjee et al. will be used [14]. In the P-N model, the dislocation core structure is described with a distribution of displacements within the core, and is determined by balancing the elastic interaction energy between the displacements in the dislocation core and the lattice restoring energy. Originally, the force equilibrium equation of the P-N model is solved for simple straight dislocations in an infinite medium. However, the complicated shape of three-dimensional dislocations makes a direct analytical solution rather difficult, and one must resort to numerical methods. The GPN model of Banerjee et al. is designed to determine dislocation core structures of complex shapes of dislocations. The basic idea in the model is to discretize the continuous distribution of displacement in the dislocation core by a number of fractional dislocations with fractional Burgers vectors. Thus, the distribution of fractional dislocations corresponds to equi-displacement contours within the dislocation core. Then the force equilibrium equation of the P-N model can be written as

$$p_i = \frac{\mu}{\pi(1-\nu)} \frac{b}{2N_f} \sum_{j \neq i}^{N_f} \frac{1}{x_j - x_i}, \tag{11}$$

where p_i is the lattice restoring stress on a fractional dislocation i, μ is the elastic shear modulus, b is the Burgers vector, N_f is the number of fractional dislocations, and x_i is the position of the i-th fractional dislocation. From Equation (11), the elastic interaction term in the P-N model is replaced with the elastic interaction between fractional dislocations. Therefore, the implementation of the P-N model within the dislocation dynamics framework is straightforward. In the dislocation dynamics method, calculation of the elastic interaction between dislocations is an essential part, which can account for the elastic interaction between fractional dislocations. The lattice restoring stress can be calculated by taking the derivative of the γ-surface energy obtained by separate atomistic calculations, such as *ab initio*, or alternatively, reliable interatomic potentials, and the force is simply added to Equation (6).

2.5. *Rigid dislocation dynamics*

To clarify the influence of dislocation line flexibility on its interaction with precipitates, we need to modify the equations of motion so as to constrain

dislocations not to bend during the interaction process. In other words, constrained dislocation dynamics will allow dislocations to move, with additional constraints on their shapes. Let us consider a dislocation lying on an x–z slip plane, and glides in the x-direction. To insure that the dislocation line remains straight, additional conditions are applied to Equation (5):

$$\frac{\mathrm{d}P_y}{\mathrm{d}t} = \frac{\mathrm{d}P_z}{\mathrm{d}t} = \frac{\mathrm{d}T_x}{\mathrm{d}t} = \frac{\mathrm{d}T_y}{\mathrm{d}t} = \frac{\mathrm{d}T_z}{\mathrm{d}t} = 0. \tag{12}$$

By the application of the above constraint, the velocity of the dislocation in both y- and z-directions are zero, and the shape is constrained to be rigidly straight. Therefore, we need to consider only the velocity of the dislocation in the x-direction. Moreover, the velocity of the dislocation in the x-direction is identical along the entire dislocation line, which reduces the degrees of freedom of the dislocation problem to only one. As a consequence, Equation (5) can be simplified to the following single degree of freedom:

$$\sum_i \sum_j K_{ij} \frac{\mathrm{d}P_x}{\mathrm{d}t} = \sum_i F_i, \tag{13}$$

where the indexes i and j are taken only for the rate of the dislocation translation in the x-direction. The implementation of rigid dislocation dynamics is an easy and straightforward implementation within the classical dislocation dynamics.

3. Dislocation-precipitate interaction

3.1. *Geometric model*

Figure 1 shows the simulation volume used in this work. The matrix material of the simulation volume is the γ'-phase, and the x-, y- and z-axes are along the crystal orientations $[\bar{1}01]$, [111], $[\bar{1}2\bar{1}]$, respectively. A straight edge super-dislocation is

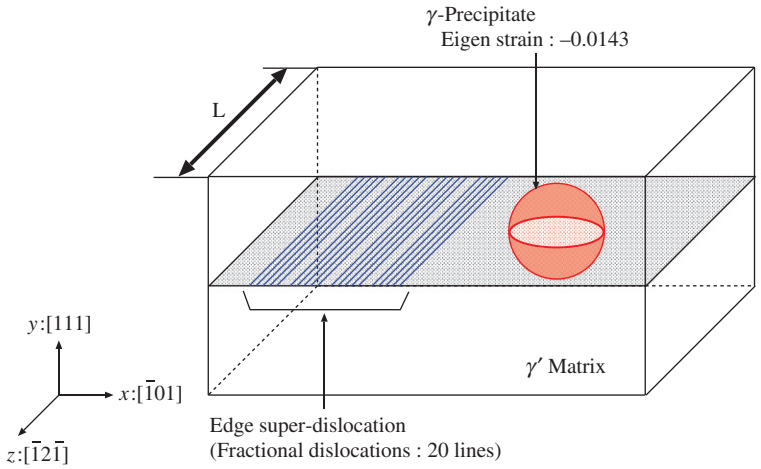

Figure 1. Schematic of simulation model for PDD simulations.

introduced into the simulation volume. The super-dislocation has a Burgers vector of $a_0^{\gamma'}[\bar{1}01]$, and is on the (111) slip plane, where a_0 is the lattice constant of the $L1_2$ ordered nickel-aluminum lattice (0.3571 nm) [20]. The core structure of the super-dislocation is represented with 20 fractional dislocations. The γ-surfaces of the γ'-phase and of the γ-precipitate are calculated using an interatomic potential developed for the nickel-aluminum binary system [20]. The lattice restoring stresses are then calculated by taking the derivative of the γ-surface, and are used as a function of position of the fractional dislocations. When part of a fractional dislocation is in the γ'-phase, the lattice restoring stress for the γ'-phase is given to that part of the fractional dislocation, whereas the lattice restoring stress for the γ-precipitate is used for the part of the fractional dislocation located inside the γ-precipitate. In reality, the γ-surface at the interface between the γ- and γ'-phase is generally different from both the γ-surface of the γ- and γ'-phases. However, for simplicity, the unique shape of the γ-surface at the interface is ignored. A spherical γ-precipitate with a coherency strain of $\epsilon = -0.0143$ is placed at the front of the super-dislocation. Periodic boundary conditions are applied in the z-direction, assuming that the dislocation is infinitely long, and the precipitate makes a 1-D periodic array in the z-direction. To move the dislocation, an external shear stress of τ_{xy} is applied to the volume, and is controlled to measure the CRSS for the interaction. The size of the simulation volume in the z-direction and the diameter of the precipitate are denoted with L and D, respectively, which are important parameters controlling the CRSS.

3.2. *γ-surface energies*

Before starting the simulation of the super-dislocation and γ-precipitate interaction, the γ-surface energies of the γ- and γ' phases must be determined, and in this work, are calculated using an interatomic potential for the nickel and aluminum binary alloy [20]. In these calculations, we used a volume with a size of $2.5 \times 12.4 \times 4.4$ nm. The x-, y- and z-axes are along the crystal orientations $[\bar{1}01]$, [111], $[\bar{1}2\bar{1}]$. Periodic boundary conditions are applied on all sides of the simulation volume. In order to make a stacking-fault in the simulation volume, a displacement of $\Delta u = a_0/6/20[\bar{1}\bar{1}2]$ is given only to the upper half of the simulation volume. Then, the motion of atoms in the x- and z-directions are constrained, and that in the y-direction is relaxed using a numerical quenching technique. The process is repeated until the total displacement given to the upper half of the simulation volume reaches $u = 20\Delta u$. Figure 2 shows the results of these calculations. Brandl et al. calculated the γ-surface energy using the *ab initio* method [21]. In order to check the accuracy, the γ-surface is also plotted in the figure. In Figure 2a, the γ-surface for nickel calculated using the interatomic potential is in excellent agreement with that obtained using the *ab initio* method. The unstable stacking fault energy is at $u = 0.27b$, whereas the intrinsic stacking-fault energy is the γ-energy at $u = 0.5b$. The dislocation core tends to have lower displacement density in the region around the unstable stacking-fault energy, and to have higher displacement density in the region around the intrinsic stacking-fault energy, resulting in the formation of an extended dislocation, which is a combination of two partial dislocations and a stacking-fault.

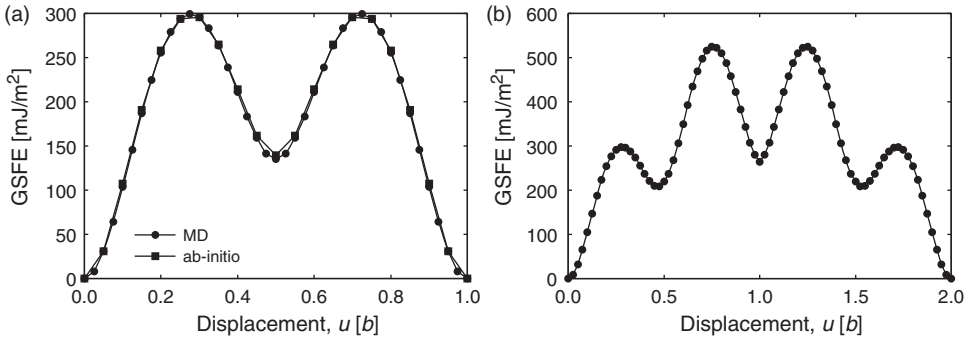

Figure 2. Generalized stacking-fault energies for the γ-(top) and γ'-(bottom) phases.

Figure 2b shows the calculated γ-surface energy for the γ'-phase, where an anti-phase boundary (APB) forms behind a leading dislocation, and a trailing dislocation terminates the APB. Thus, dislocations must move in pairs in a *super-dislocation* configuration. In the present calculation of the γ-surface energy for the γ'-phase, the maximum displacement is $40\Delta u$, which is twice that given to the atomic volume in the γ-surface calculation in the γ-phase. In the figure, there are two local maxima in the γ-surface energy, resulting in the formation of an extended dislocation in the super-dislocation core. Moreover, there are two local minima at $u = 0.42b$ and $1.58b$, which correspond to the complex stacking-fault between two partial dislocations of the extended dislocation, and the APB between two super-partials of the super-dislocation. The complex stacking-fault and APB energies are $202\,\mathrm{mJ/m^2}$ and $252\,\mathrm{mJ/m^2}$ [20], whereas the experimental results of the energies are $235\,\mathrm{mJ/m^2}$ and $175\,\mathrm{mJ/m^2}$ [22], respectively.

4. γ-precipitate strengthening

γ-precipitate strengthening in nickel-based superalloys is a result of several mechanisms that operate concurrently. Following Ardell [1], chemical strengthening and modulus hardening do not substantially affect the overall strength of the alloy. Therefore, in this work, we focus only on the influence of the stacking-fault and coherency strain mechanisms, and study the strengthening effect of each one separately. The main focus will thus be on the influence of the dislocation line flexibility, and the details of its core structure on the overall strength. Finally, the mechanism of γ-precipitate strengthening, which can be defined as the mixed strengthening of the stacking-fault and coherency strain, will be fully explored.

4.1. *Coherency strengthening*

Gerold and Haberkorn developed an analytical solution to the increase in the CRSS as a result of coherency interaction between a dislocation and a precipitate [4]. To obtain a closed form solution, they assumed that the dislocation shape is straight, and that the dislocation core is infinitely narrow (i.e. the displacement field has

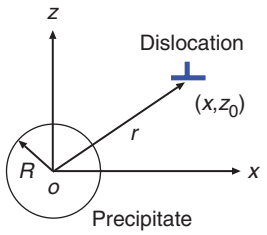

Figure 3. Coordinate system for calculations of precipitate coherency strengthening.

a discontinuity at the line). Let us now consider an edge dislocation on the x–y slip plane located at z_0 and gliding in the x-direction, together with a precipitate of radius R and a coherency strain $\in$, as shown in Figure 3. When the dislocation line is at a position (x, z_0), it suffers an interaction force $K(x)$ from the precipitate, which can be calculated by integrating the Peach–Koehler force produced by the precipitate along the dislocation line (y-direction), and is given as

$$\begin{aligned} K(x) &= b\int_{-\infty}^{\infty} \tau_{xz}(x, y, z_0)\,\mathrm{d}y \\ &= \frac{8}{3}\frac{1+\nu}{1-\nu}\frac{\mu b|\in|R^3 x_0 z_0}{(x_0^2+z_0^2)^2} \\ &\quad\times\left\{1-\frac{y_0(2R^2+x^2+z_0^2)}{2R^3}\right\} \\ y_0^2 &= \begin{cases} R^2-\left(x^2+z_0^2\right) & (x^2+z_0^2<R^2) \\ 0 & (x^2+z_0^2\geq R^2). \end{cases} \end{aligned} \tag{14}$$

The CRSS can be calculated finding the maximum interaction force, and given as

$$\tau_{\mathrm{crss}} = \frac{K(x)|_{\max}}{bL}. \tag{15}$$

To investigate the influence of coherency strengthening alone, the γ-surface energy for the γ'-phase is used for both matrix and precipitate. The diameter of the γ-precipitate is fixed to 8 nm, and the position of the slip plane is changed from upper (the precipitate comes into the compression side of dislocation) to lower (into the tension side) positions with respect to the mid-plane of the precipitate. The size of the simulation volume is taken as $50\times50\times20$ nm. Figure 4 shows successive snapshots of the dislocation geometry during its interaction with the γ-precipitate. Note that each line represents a constant displacement contour within the dislocation core, with values in the range $(0, b)$. The fractional dislocations (each representing a constant displacement contour) cluster into four groups, which respectively correspond to the leading and trailing partials of the super-partials of the super-dislocation. In Figure 4a, where the slip plane is 3 nm above the mid-plane, the central part of the dislocation is immobilized by the coherency strain at the front of the precipitate. In this case, most of the precipitate is on the compression side of the super-dislocation, and the precipitate has a negative coherency strain. Therefore, the super-dislocation and the precipitate have a repulsive interaction force.

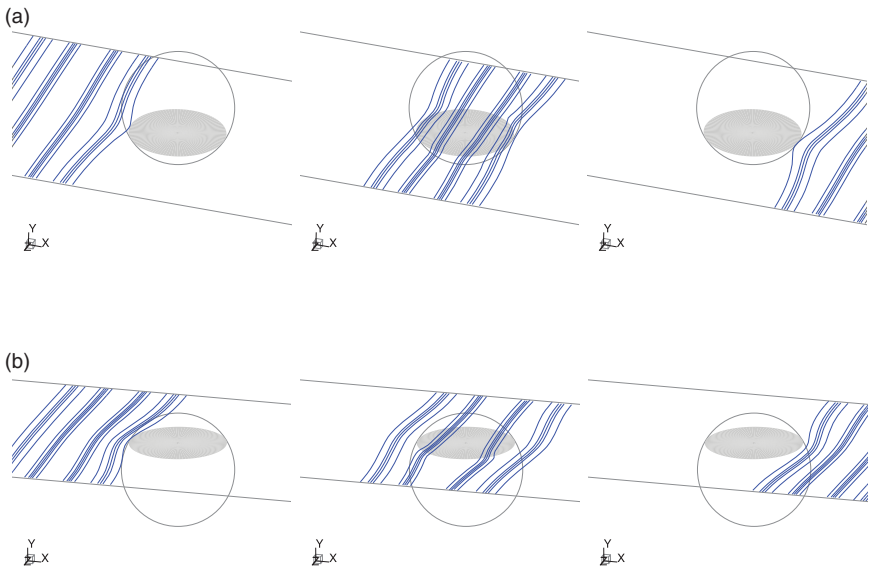

Figure 4. Snapshots of the dislocation core structure during the interaction between a super-dislocation and a γ-precipitate accounting only for precipitate coherency strain. (a) Slip plane position: 3 nm above the mid-plane; (b) slip plane position: 3 nm below the mid-plane.

Upon increasing the applied shear stress, the leading super-partial starts to cut through the precipitate. Once the dislocation moves inside the precipitate, it is strongly pushed to the outside of the precipitate by the interaction. After breaking away from the precipitate, the super-dislocation is still influenced by a repulsive interaction force that enhances its glide. On the other hand, as shown in Figure 4b, the central part of the super-dislocation spontaneously dissociates inside the precipitate, because most of the precipitate is on the tension side of the dislocation and the precipitate has an attractive interaction force with the super-dislocation. Thus, the super-dislocation tends to stay inside the precipitate so that the maximum interaction appears at the center of the precipitate. When the applied shear stress reaches the CRSS, the dislocation can finally cut through the precipitate.

Figure 5 shows the increase in the CRSS due to the precipitate coherency strain. In the figure, the CRSS is calculated using four different computational methods: (1) PDD, (2) PDD with the GPN model, (3) rigid PDD, and (4) rigid PDD with the GPN model, and the results are all plotted in the same figure. In order to compare the simulation results to classical analytical solutions [4], the CRSS calculated by Equation (15) is also plotted. It is observed that when the dislocation is placed at the center of the γ-precipitate, the CRSS does not increase, while the maximum CRSS occurs when the dislocation slip plane is at $z/R = \pm 0.75$. A shear stress must be applied to the dislocation to overcome the coherency strain field, even when the dislocation does not directly cut the precipitate, because of the long-range nature of the strain field, as can be seen in the figure. The results of calculations using the full PDD method, the rigid PDD method, and those of Equation (15) show excellent agreement. However, the results of the (rigid) PDD with the GPN model differ

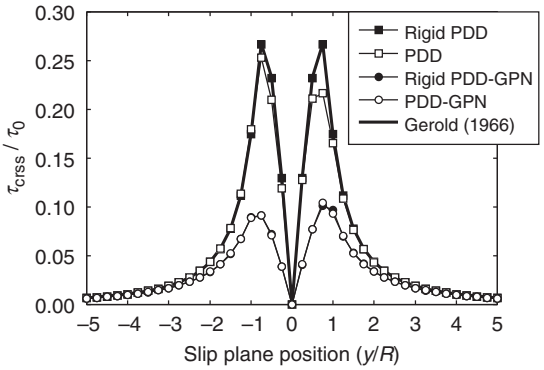

Figure 5. The increase in the CRSS as a function of the slip plane position as a result of coherency strengthening by the precipitate strain field.

significantly, particularly when the dislocation is on the slip plane at $z/R = \pm 0.75$. Since Equation (15) is derived with the assumptions that dislocation is perfectly straight, and that the core structure is ignored, the agreement between the rigid PDD method and Equation (15) is reasonable. Since the results of the full PDD simulation are also identical to those of the rigid PDD method, we conclude that the influence of the dislocation line flexibility on the coherency strengthening mechanism must be negligibly small. Thus, the significant difference between the results of Equation (15) and those of the (rigid) PDD with the GPN model must be attributed to the influence of the core structure of the dislocation.

The present simulation results will now be utilized to extend the applicability of Equation (15) by incorporating the influence of the core structure of dislocations as they interact with precipitates. Referring to the coordinate system of Figure 3, we decompose the super-dislocation into four partial dislocations D_i, where the positions of each partial dislocation x_i are assumed to be $x_2 = x_1 + w_c$, $x_3 = x_2 + w_a$ and $x_4 = x_3 + w_c$, where w_c and w_a are the widths of the complex stacking-fault between two partial dislocations of a super-partial dislocation, and the anti-phase boundary between the super-partial dislocations. For simplicity, we consider an infinitely long straight edge super-dislocation in an infinite isotropic elastic body, and include the elastic interaction between the partial dislocations as well as the energy of the complex stacking-fault and anti-phase boundaries. The widths w_c and w_a can be calculated by solving the following equilibrium equations:

$$\frac{Gb^{e2}}{2\pi(1-\nu)}\left(\frac{1}{w_c}+\frac{1}{w_c+w_a}+\frac{1}{2w_c+w_a}\right) + \frac{Gb^{s2}}{2\pi}\left(-\frac{1}{w_c}+\frac{1}{w_c+w_a}-\frac{1}{2w_c+w_a}\right) = \gamma_c \tag{16}$$

$$\frac{Gb^{e2}}{2\pi(1-\nu)}\left(-\frac{1}{w_c}+\frac{1}{w_a}+\frac{1}{w_c+w_a}\right) + \frac{Gb^{s2}}{2\pi}\left(\frac{1}{w_c}-\frac{1}{w_a}+\frac{1}{w_c+w_a}\right) = \gamma_a - \gamma_c. \tag{17}$$

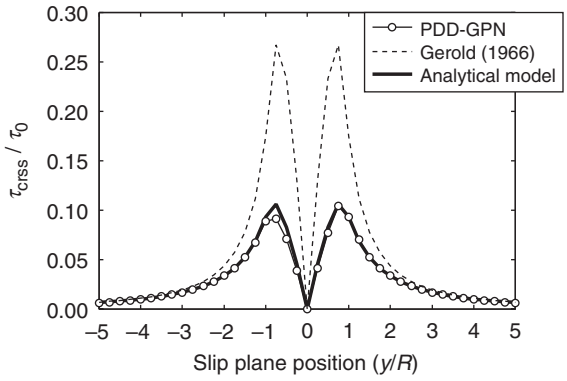

Figure 6. The increase in the CRSS as a function of the slip plane position as a result of coherency strengthening by the precipitate strain field, calculated by direct numerical simulation, and compared to the results of Gerold and the proposed analytical model given by Equation (18).

Similar to Equation (15), taking the summation of the $K(x_i)$, and finding the maximum, the CRSS can be calculated as

$$\tau_{\text{crss}} = \frac{\sum_i^4 K(x_i)|_{\max}}{bL}. \tag{18}$$

Figure 6 shows the results of the PDD with the GPN model simulation, and compared to calculations based on Equation (15) as well as Equation (18). The CRSS increase calculated by Equation (18) is considerably smaller than those calculated by Equation (15), which is in excellent agreement with the numerical simulation results. Thus, it is clear that the influence of the core structure of dislocations on coherency strengthening is very significant (the maximum is lowered by a factor of almost 3), and that the influence can be accurately accounted for using the proposed Equation (18).

4.2. *Stacking-fault strengthening*

If the energy of the stacking-fault between two partial dislocations is larger inside the precipitate than in the matrix, an additional shear stress must be applied on the dislocation to overcome that energy difference, $\Delta\gamma$, and allow the dislocation to cut through the precipitate. Nembach derived an analytical expression to calculate the required shear stress due to stacking-fault strengthening [3]. An extended dislocation, composed of two partial dislocations and a stacking-fault in-between, was considered, and the length of each partial dislocation inside the precipitate, $L(x)$, was used to find the interaction force between the precipitate and the dislocation K:

$$K(x) = (L(x) - L(x+w))\Delta\gamma, \tag{19}$$

where w is the distance between the leading and trailing partial dislocations, $L(x)$ and $L(x+w)$ are the lengths of the leading and trailing partial dislocations, at x

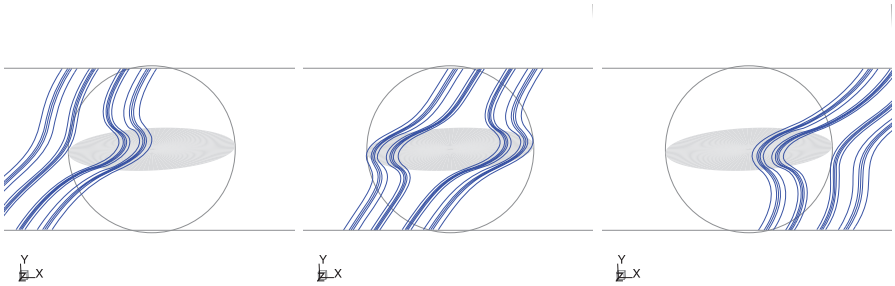

Figure 7. Snapshots of the interaction between a super-dislocation and a γ-precipitate as a result of differences in the stacking-fault between the matrix and precipitate (stacking-fault strengthening).

and $x + w$, inside the precipitate, respectively. The CRSS can be calculated by finding the maximum interaction force, and is given by [3]

$$\tau_{\text{crss}} = \frac{K(x)|_{\max}}{bL}. \tag{20}$$

To determine the accuracy of the analytical solution of Nembach, and any possible effects of the exact core structure on stacking-fault strengthening, we perform numerical simulations where the influence of the coherency strain is removed by setting $\epsilon = 0$, and that of the stacking-fault is accounted for by giving the γ-surface information of both the γ- and γ'-phases. When part of the fractional dislocation is located in the γ-phase, the lattice restoring stress of γ-phase, which can be calculated from the γ-surface of γ-phase, is given to that part, whereas the lattice restoring stress of the γ'-phase is given to the part of the fractional dislocation inside the γ'-phase. The simulation volume used here is identical to that used in the previous section, and the diameter of the precipitate is changed in the range from 2 to 30 nm. The slip plane position of the super-dislocation is fixed at the center of the precipitate. Figure 7 shows snapshots of the dislocation configuration as it interacts with the precipitate (here the precipitate diameter is 16 nm). It is clear that the super-dislocation and the precipitate are attracted to one another, and that the super-dislocation is first absorbed by the precipitate. When the dislocation enters the γ-precipitate, the anti-phase boundary disappears, and the complex stacking fault is changed to an intrinsic stacking-fault, which has a lower energy than the complex stacking-fault. Thus, the super-dislocation tends to be attracted inside the precipitate to reduce the interaction energy. Increasing the externally applied shear stress, the dislocation gradually starts to bow-out, and finally breaks away from the precipitate when the applied shear stress reaches its critical value (the CRSS).

Figure 8 shows the results of the numerical simulations (both the full PDD-GPN model, and the rigid PDD-GPN model). Also, the results of Equation (20) are plotted for comparison. As the precipitate diameter increases, the CRSS also increases, which is a consequence of an increase in the stacking-fault area between partials when they enter into the precipitate. Additionally, the results of all numerical simulations with both methods, and those of Equation (20), are within a few percent.

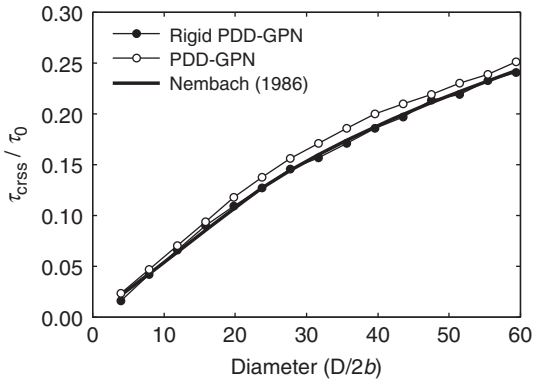

Figure 8. Dependence of the CRSS on precipitate diameter for the stacking-fault strengthening mechanism alone.

Therefore, Equation (20) reasonably accounts for stacking-fault strengthening, as long as the dislocation core can be described by two isolated peaks of displacement distributions (i.e. well-isolated partials). The core structure of dislocations is then an important factor in determining the CRSS, and Equation (20) can be used in cases where the two partial dislocations are well-isolated.

4.3. *Mixed strengthening*

Precipitate strengthening is a result of several factors, such as the stacking-fault, coherency, and modulus strengthening mechanisms. However, in the present case of nickel-based superalloys, precipitate strengthening is primarily due to the stacking-fault and the coherency strengthening mechanisms, because the difference in the elastic moduli between the matrix and precipitate is very small. Therefore, we describe here γ-precipitate strengthening as a combination of the stacking-fault and coherency strengthening effects, and propose a method to evaluate the overall CRSS increase when the two mechanisms are operating simultaneously. The simulation volume and boundary conditions used in this section are the same as those used in previous simulations, while the diameter of the γ-precipitate is fixed to 8 nm. Figure 9 shows the dependence of the CRSS on the location of the slip plane. As can be seen, in the stacking-fault strengthening mechanism, the distribution of the CRSS is symmetric about the center of the precipitate, and shows a maximum at the center. When the position of the slip plane is outside the precipitate, there is no increase in the CRSS increase, as expected.

It is clear that the CRSS outside the precipitate is identical to that due to the coherency strain mechanism, while inside the precipitate both the coherency and stacking-fault mechanisms operate simultaneously. In fact, as the slip plane gets closer to the precipitate mid-plane, the influence of coherency strain diminishes, while stacking-fault strengthening reaches its maximum. However, the distribution of the CRSS when the two mechanisms operate simultaneously (mixed strengthening) has a complex structure as a function of the slip plane position, and its

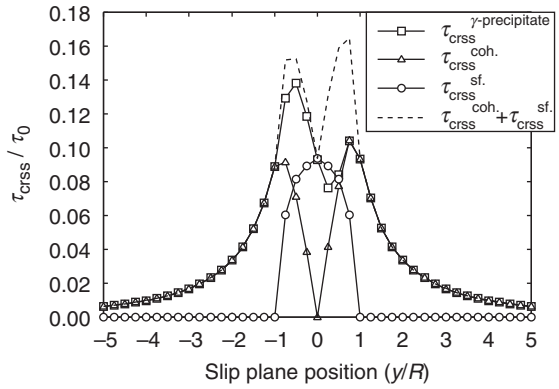

Figure 9. The CRSS as a function of the slip plane position for coherency (triangles) and stacking-fault (open circles), simple summation (dashed line), and full calculation (open squares).

maximum cannot be simply the sum of the two independent maxima for each mechanism separately, a procedure that is common in precipitation hardening estimates. To further demonstrate this point, we also used a simple summation rule for the CRSS resulting from the stacking-fault and the coherency strengthening mechanisms, and plot the results in Figure 9 (dashed line). Here, the simple sum does not represent overall precipitate hardening very well. When the dislocation is on the compression side of the precipitate, the stacking-fault shrinks, while it widens when it is on the tension side, giving rise to the asymmetric distribution of the CRSS as a function of the slip plane position when the two mechanisms operate simultaneously, a result that cannot be predicted by simple addition of the two effects.

The interaction forces between the super-dislocation and the precipitate, using Equations (18) and (20), are calculated and plotted in Figure 10 as functions of the dislocation position from the precipitate center, when the slip plane is at -2 nm from the mid-plane. It is observed that the peaks of the interaction force due to the stacking-fault and the coherency mechanisms appear at different positions, suggesting that the summation of the CRSS (which is equivalent to summing the maximum forces) is not a good way to represent the true spatial dependence of the CRSS for mixed strengthening. The figure also shows the total interaction force due to the stacking-fault and coherency strengthening mechanisms as a function of dislocation position. Since the dislocation has to overcome the maximum total interaction force, we calculated the CRSS at different slip planes, using only the maximum interaction force, and we show the results in Figure 11. We compare here the CRSS as a function of the slip plane position, using the full PDD-GPN model, and comparing it to the more simplified model of using only the maximum value of the calculated shear stress at each slip plane. These two methods show excellent agreement, indicating that, in order to calculate the CRSS for mixed strengthening, the maximum interaction force for a given slip plane can be first computed and stored, and then used in subsequent DD simulations without having to perform detailed simulations.

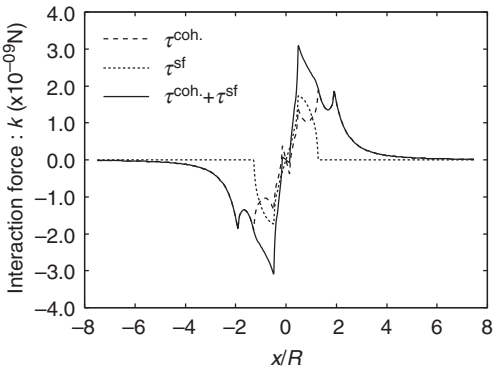

Figure 10. Dependence of the coherency and stacking-fault interaction forces on the dislocation position, when it lies on a slip plane at −2 nm, which is half of the precipitate radius, from the mid-plane.

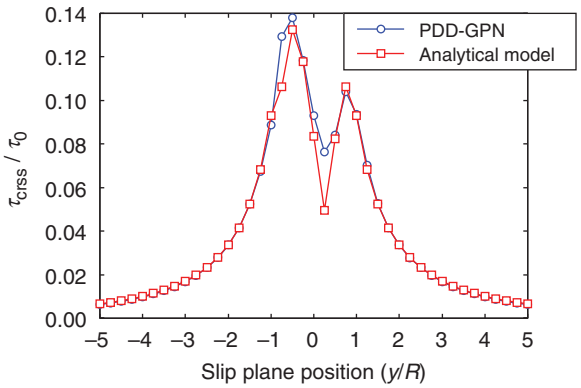

Figure 11. Comparison of the dependence of the CRSS on the slip plane position. Numerical simulations with the full PDD-GPN model are compared with the analytical model. The results of the analytical model are given as the maximum total interaction force of the stacking-fault and the coherency strengthening.

5. Conclusions

A computational method for investigations of the role of dislocation flexibility and the dislocation core structure on the dislocation–precipitate interaction has been developed. The method is a combination of the PDD, with lattice resistance to dislocation motion obtained from the GPN model. To quantitatively evaluate the influence of dislocation flexibility on its interaction with precipitates, we added a constraint condition on the dislocation shape in PDD simulations. The method allows us to simulate the dynamics of rigid dislocations in internal and external stress fields. Using the computational method, we studied γ-precipitate strengthening in nickel-based superalloys, and determined the roles played by the dislocation line flexibility and its core structure. Conclusions of the present study are summarized in the following:

(1) Using four different interaction models (PDD, rigid PDD, PDD with GPN, and rigid PDD with GPN), it is found that the influence of dislocation line flexibility is negligibly small, whereas the dislocation core structure is found to play a major role in determining the CRSS.
(2) An analytical equation for coherency strengthening is revised to incorporate the dislocation core information into the evaluation of the CRSS. The revised equation reproduces very well the results of detailed PDD simulations with the GPN model.
(3) Again, the influence of the dislocation line flexibility on the stacking-fault strengthening is found to be negligible.
(4) An analytical equation, which is derived with a dislocation model composed of two partial dislocations and a stacking-fault in-between, precisely reproduces the CRSS of the stacking-fault strengthening mechanism.
(5) The summation of the CRSSs of the stacking-fault and coherency strengthening mechanisms is found to give unacceptable values of the CRSS.
(6) Taking the summation of the shear stresses of the stacking-fault and coherency strengthening mechanism, and finding the maximum of the total interaction force reproduces very well the CRSS for mixed strengthening. The developed method is a promising approach in determining the CRSS of mixed types of precipitation strengthening mechanisms, without the detailed simulations.

Acknowledgement

This research is supported by the US Air Force Office for Scientific Research (AFOSR), Grant No. FA9550-07-1-0396 at UCLA.

References

[1] A.J. Ardell, Metall. Trans. A 16 (1985) p.2131.
[2] P.B. Hirsch and A. Kelly, Phil. Mag. 12 (1965) p.881.
[3] E. Nembach, Scripta Metall. 20 (1986) p.763.
[4] V. Gerold and H. Haberkorn, Physica Status Solidi 16 (1966) p.675.
[5] M.K. Miller, Micron 32 (2001) p.757.
[6] M. Nemoto, W.H. Tian, K. Harada, C.S. Han and T. Sano, Mater. Sci. Eng. A 152 (1992) p.247.
[7] N.M. Ghoniem, S.-H. Tong and L.Z. Sun, Phys. Rev. B 61 (2000) p.913.
[8] E. van der Giessen and A. Needleman, Model. Simul. Mater. Sci. Eng. 3 (1995) p.689.
[9] E. Weygand, L.H. Friedman, E. Van der Giessen and A. Needleman, Model. Simul. Mater. Sci. Eng. 10 (2002) p.437.
[10] A. Takahashi and N.M. Ghoniem, J. Mech. Phys. Solids 56 (2008) p.1534.
[11] Y. Xiang, D.J. Srolovitz, L.-T. Cheng and E. Weinan, Acta Mater. 52 (2004) p.1745.
[12] B. Devincre, L.P. Kubin, C. Lemarchand and R. Madec, Mater. Sci. Eng. A 309–310 (2001) p.211.
[13] S.I. Rao, T.A. Parthasarathy, D.M. Dimiduk and P.M. Hazzledine, Phil. Mag. 86 (2004) p.3195.
[14] S. Banerjee, N.M. Ghoniem, G. Lu and N. Kioussis, Phil. Mag. 87 (2007) p.4131.

[15] M.A. Shehadeh, G. Lu, S. Banerjee, N. Kioussis and N.M. Ghoniem, Phil. Mag. 87 (2007) p.1513.
[16] T. Mura, *Micromechanics of Defects in Solids*, Martinus Nijhoff, Dordrecht, 1982.
[17] J.D. Eshelby, Proc. Roy. Soc. A 241 (1957) p.376.
[18] R. Peierls, Proc. Phys. Soc. 52 (1940) p.34.
[19] F.R.N. Nabarro, Proc. Phys. Soc. 59 (1947) p.256.
[20] Y. Mishin, Acta Mater. 52 (2004) p.1451.
[21] C. Brandl, P.M. Derlet and H. Van Swygenhoven, Phys. Rev. B 76 (2007) p.054124.
[22] H.P. Karnthaler, E.Th. Muhlbacher and C. Rentenberger, Acta Mater. 44 (1996) p.547.